Calculation of the magnetic anisotropy with projected-augmented-wave methodology and the case study of disordered $Fe_{1-x}Co_x$ alloys

Soner Steiner,[1] Sergii Khmelevskyi,[1,2] Martijn Marsmann,[1] and Georg Kresse[1]
[1]*Institut für Materialphysik and Center for Computional Materials Science, Universität Wien, Sensengasse 8, 1090 Vienna, Austria*
[2]*Center for Computational Materials Science, Vienna University of Technology, Wiedner Hauptstrasse 8, 1040 Vienna, Austria*
(Received 28 December 2015; revised manuscript received 15 May 2016; published 23 June 2016)

The magnetic anisotropy energy of tetragonally distorted disordered alloys $Fe_{1-x}Co_x$ is calculated by two different virtual crystal approximation methods and an averaged supercell method within the projected-augmented-wave (PAW) methodology and the magnetic force theorem. The details of the spin-orbit coupling implementation in the PAW methodology are given. We compare our results to the recent coherent potential approximation (CPA) studies, results of full potential calculations, and to the available experiments.

DOI: 10.1103/PhysRevB.93.224425

I. INTRODUCTION

The magnetic anisotropy energy (MAE) of transition metal intermetallics and alloys is a key property determining the materials performance as a hard magnet in modern electronic memory devices [1–5]. With the development of highly efficient band structure codes, extensive efforts have been made to calculate the magnetic anisotropy within the the local spin density approximation (LSDA) [6] and the corresponding generalized gradient approximation in various bulk, surface, and multilayer materials. In transition metal systems, where the magnitude of the anisotropy is much smaller than in the rare-earths materials, the MAE appears only at second and higher orders of the perturbation expansion over the spin-orbit coupling (SOC) imposing stringent requirements for the computational accuracy. First-principles calculations of the MAE within a relativistic band structure theory based on LSDA were successful in d-transition metal based ferromagnetic multilayers [7,8], surfaces and overlayers [9], low-dimensional nanostructures [10], and adatoms on surfaces [11]. In these systems, the MAE is two or three orders of magnitude larger than in the bulk elemental transition metals Fe, Ni, and Co. For elemental cubic metals or hcp Co, where the MAE magnitude is of the order of few μeV/atom, the results of first-principles relativistic simulations are still very controversial [7,12]. However, the LSDA predicts the anisotropy well in ordered bulk alloys and in intermetallics where the anisotropy of the magnetic 3d-metal is enhanced due to for example lower crystal symmetry (e.g., tetragonal distortion) and/or another heavy element with strong SOC (e.g., Pt, Bi, etc.).

One of the most prominent examples of the systems where the MAE has been extensively studied in recent decades are the binary Fe-Co alloys. Since Burkert *et al.* [13] have shown from a first-principles calculation a very strong anisotropy enhancement in these alloys due to a tetragonal distortion, a number of studies has been done to investigate thin films of this material (see recent paper by Şaşıoğlu *et al.* [14], and references therein). On the basis of the calculations utilizing the coherent potential approximation (CPA) [15] for disordered alloys in the framework of the atomic sphere approximation (ASA), it has been shown that the MAE in tetragonal FeCo significantly reduces as atomic disorder increases. Neise *et al.* [16] investigated the magnetic anisotropy in the distorted Fe-Co alloys using a full potential methodology in the framework of the linear combination of atomic orbitals (FPLO) methods [17]. To model the atomic disorder they used an averaging of the magnetic anisotropy calculated over the supercells with random distributions of Fe and Co atoms for three alloy compositions: $Fe_{1-x}Co_x$ with $x = 0.5$, $x = 0.625$, and $x = 0.75$. They also found that the atomic disorder leads to a decrease of the magnetic anisotropy compared to the atomically ordered alloys. Both methods CPA [15] and supercell averaging [16] predict the maximal MAE for the tetragonal distortion c/a around 1.25 and for the Co concentration at compositions around $x = 0.6$. In both studies it has been demonstrated that the simple standard virtual crystal approximation (VCA) gives a rather high value of the MAE compared to the more refined methods of treatment of the chemical disorder.

Although the CPA is often very successful for the description of the electronic structure of the disordered alloys, it is an effective medium theory that does not destroy the local symmetry around a given atomic site. Since the SOC on a given-atomic site may strongly depend on the symmetry of the local atomic environment of Fe or Co, the MAE might be very sensitive on how alloy averaging is performed. The investigation of this topic is one of the issues of the present work. To compare the CPA-ASA results with averaging over the supercells more thoroughly, we investigate in this work a full range of $Fe_{1-x}Co_x$ alloy compositions from $x = 0$ to $x = 1$. We will also compare the supercell averaging results for the MAE with the standard VCA [18–22] and a variant recently proposed [23]. This variant is not necessarily an improvement, but rather a convenient description within the PAW method, since it eliminates the need to construct pseudopotentials for every considered concentration. In the remaining text we will refer to this method as VCA2.

Another issue of the present work is motivated by the growing number of MAE calculations for various transition metal systems performed within the PAW methodology with spin-orbit coupling as implemented in the Vienna *ab initio* simulation package (VASP) [24]. In this paper we provide a description of the details of the SOC implementation in the VASP code. The tetragonally distorted Fe-Co alloys are ideal examples to check the VASP accuracy for MAE calculations by comparing to other methodologies and experimental results. In particular, it has been found in Refs. [13,15] that the VCA overestimates the MAE and this is fully confirmed in the

present study using both VCA, as well as VCA2 calculations. Using random supercells, we also obtain excellent agreement with previously performed CPA calculations [15]. This proves, hopefully beyond doubt, that magnetic anisotropy calculations are feasible within the PAW methodology and compare very well with other methods.

II. SPIN-ORBIT COUPLING IMPLEMENTATION IN THE PAW METHOD

In the projector-augmented-wave (PAW) method of Blöchl [25], the one-electron orbitals ψ_n are written as

$$|\psi_n\rangle = |\widetilde{\psi}_n\rangle + \sum_i (|\phi_i\rangle - |\tilde{\phi}_i\rangle)\langle\tilde{p}_i|\widetilde{\psi}_n\rangle. \tag{1}$$

The pseudo (PS) orbitals $\widetilde{\psi}_n$ are the variational quantities of the PAW method, and are expanded in plane waves. ϕ_i and $\widetilde{\phi}_i$, the all-electron (AE) and pseudo partial waves, are additional local basis functions that are nonzero only within the PAW spheres centered at the atomic sites. In the interstitial region between the PAW spheres, therefore, the true one-electron orbitals ψ_n are identical to the PS orbitals $\widetilde{\psi}_n$. Inside the PAW spheres the PS orbitals are only a computational tool and a bad approximation to the true wave functions, since not even the norm of the true wave function is reproduced. In all practical implementations of the PAW method, the AE partial-waves ϕ_i are chosen to be solutions of the spherical (scalar relativistic) Schrödinger equation for a *nonspinpolarized atom* at a specific energy ε_i in the valence regime, and for a specific angular momentum l_i. The PS partial waves $\widetilde{\phi}_i$ are equivalent to their AE counterparts outside a core radius r_c and match continuously onto ϕ_i inside this radius. The projector functions $\widetilde{p}_i$ are constructed to be dual to the PS partial waves, i.e.,

$$\langle\widetilde{p}_i|\widetilde{\phi}_j\rangle = \delta_{ij}. \tag{2}$$

For a comprehensive description of the implementation of the PAW method in VASP we refer the reader to the paper of Kresse and Joubert [26] and references therein.

It is straightforward to show that within the PAW method any (semi)-local operator O acting on ψ_n can be written as a pseudo operator $\widetilde{O}$ that acts on the PS orbitals $\widetilde{\psi}_n$ [25]:

$$\widetilde{O} = O + \sum_{ij} |p_i\rangle(\langle\phi_i|O|\phi_j\rangle - \langle\tilde{\phi}_i|O|\tilde{\phi}_j\rangle)\langle p_j|. \tag{3}$$

The spin-orbit coupling (SOC) acts predominantly in the immediate vicinity of the nuclei and we assume its effects to be negligible outside of the PAW spheres. Under that assumption and provided that the PS partial waves $\tilde{\phi}_i$ form a complete basis set within the PAW spheres, the first and third terms on the right-hand-side of Eq. (3) cancel exactly, and the contribution of the SOC to the PAW Hamiltonian reduces to the AE one-center contribution:

$$\widetilde{H}_{\mathrm{SO}} = \sum_{ij} |p_i\rangle\langle\phi_i|H_{\mathrm{SO}}|\phi_j\rangle\langle p_j|. \tag{4}$$

In the zeroth-order-regular approximation, H_{SO} is given by [27]

$$H_{\mathrm{SO}}^{\alpha\beta} = \frac{\hbar^2}{(2m_e c)^2}\frac{K(r)}{r}\frac{dV(r)}{dr}\vec{\sigma}^{\alpha\beta}\cdot\vec{L}. \tag{5}$$

Here the angular momentum operators $\vec{L}$ is defined as $\vec{L} = \vec{r}\times\vec{p}$, and $\vec{\sigma} = (\sigma_x,\sigma_y,\sigma_z)$ are the (2×2) Pauli spin matrices, $V(r)$ is the spherical part of the effective AE potential within the PAW sphere, and

$$K(r) = \left(1 - \frac{V(r)}{2m_e c^2}\right)^{-2}. \tag{6}$$

Using $\phi_i(\mathbf{r}) = R_i(|\mathbf{r}|)Y_{l_i m_i}(\hat{\mathbf{r}})$ we rewrite Eq (5) as

$$\widetilde{H}_{\mathrm{SO}}^{\alpha\beta} = \frac{\hbar^2}{(2m_e c)^2}\sum_{ij}|\tilde{p}_i\rangle R_{ij}\vec{\sigma}_{\alpha\beta}\cdot\vec{L}_{ij}\langle\tilde{p}_j|, \tag{7}$$

where

$$R_{ij} = 4\pi\int_0^{r_c} R_i(r)\frac{K(r)}{r}\frac{dV(r)}{dr}R_j(r)dr \tag{8}$$

and

$$\vec{L}_{ij} = \langle Y_{l_i m_i}|\vec{L}|Y_{l_j m_j}\rangle, \tag{9}$$

and Y_{lm} are real spherical harmonics.

The action of the SOC operator on the PS orbitals is evaluated as

$$|\widetilde{\psi}_n^{\alpha}\rangle = \sum_{\alpha\beta}\widetilde{H}_{\mathrm{SO}}^{\alpha\beta}|\widetilde{\psi}_n^{\beta}\rangle, \tag{10}$$

where α and β label the spin-up and spin-down components of the two-component spinor wave functions necessary to describe noncollinear magnetism [28].

III. COMPUTATIONAL DETAILS

In this work the magnetic anisotropy of $Fe_{1-x}Co_x$ was calculated in three different ways. First, the standard VCA pseudopotential PAW procedure was used. This is applicable to neighboring elements in the periodic table, say Fe and Co. In this case, a potential is created for a fictitious element with a valency between Fe and Co. In many cases, such interpolations have been proven to be successful for the calculations of various alloys properties [18–22]. The main advantage of the VCA method is its simplicity and computational efficiency explaining its wide spread use compared to full potential Green's function based methods. Second, we use the VCA method of Ref. [23] (VCA2) developed for the pseudopotential methodology. In this VCA, a specific concentration of $Fe_{1-x}Co_x$ is obtained placing Fe and Co PAW potentials at the same lattice site, and weighting the PAW potential of Co by a factor of x and the PAW potential of Fe by a factor of $1-x$. The applicability of the VCA2 within the PAW methodology was recently demonstrated in [29] for Sn_xGe_{1-x} alloys. Third, we used a supercell with 16 atomic sites to describe the chemical disorder by means of averaging. The positions of the Fe and Co atoms in the supercell are randomized and eight different SCs are used for calculating the MAE by averaging. Note that we took a completely random set of the supercells without the optimization proposed in Refs. [16,30].

For all three models we used the equilibrium volume of the bcc structure calculated using the VCA and kept the volume constant while varying the c/a ratio of the bct unit cell of $Fe_{1-x}Co_x$ from 1.0 to 1.4. In fact, earlier studies by Neise *et al.* [16] and Burkert *et al.* [13] have shown negligible effects of the volume relaxation on the calculated value of the MAE in distorted Fe-Co systems.

We use the Vienna *ab initio* simulation package (VASP) [24] within the projector-augmented-plane-wave (PAW) method [25,26]. All calculations were performed using the PBE GGA (Perdew-Burke-Ernzerhof generalized gradient approximation) [31] functional. Additionally for some points PAW LDA (local density approximation) [32] calculations were done. We note that, in the LDA, we interpolated the correlation in the same way as the exchange from the nonmagnetic to the ferromagnetic regime, whereas in the PBE as well as in the LDA calculations of Ref. [15] the interpolation scheme of Vosko, Wilk, and Nusair is used [33]. We will merely use the LDA to demonstrate that the final results are very sensitive to computational details, in particular in the Co rich regime. The default energy cutoff of 280 eV was used for all calculations. The k-point integration was done using the tetrahedron method with Blöchl corrections [25].

The MAE was determined using the so-called magnetic force theorem [7,34], by performing a fully self-consistent calculation for the collinear case and, in the second step, freezing the potential charge density for different orientations of the magnetization direction and then taking the energy differences $K_u = E^{[100]} - E^{[001]}$, where $E^{[100]}$ and $E^{[001]}$ are the energies with the magnetization in the [100] and [001] directions of the bct structure, respectively.

We achieve a convergence of the MAE energy of about 0.1 μeV/atom using 4096 k points over the complete BZ for the VCA and VCA2 cases and 512 k points for the SC. The convergence tests have been performed for up to 32 768 k points for VCA and VCA2 and using 4096 k points for the supercells.

IV. RESULTS AND DISCUSSION

The equilibrium lattice constants of the nondistorted bcc $Fe_{1-x}Co_x$ alloys and magnetic moments of the fictitious atoms obtained with VCA calculations are presented in Fig. 1. The corresponding unit cell volumes were used further in calculations of tetragonal bct structures with varying c/a ratios including supercell calculations. Interesting to note that the lattice constant increases up to the concentration $x = 0.2$ and then decreases with increasing Co concentration. This agrees with experimental observations [35]. Clearly the magnetic moments follow the same trend as the volume.

The dependence of the MAE of the bct alloy $Fe_{1-x}Co_x$ on the chemical composition and on the a/c ratio is shown in Fig. 2 calculated with VCA, VCA2, and the 16 atoms supercell models. Both VCA results agree well with earlier VCA calculations [13,15,16]. The MAE has a maximum at about $x = 0.6$ and $c/a = 1.25$. There is no essential difference between VCA and VCA2 results. Although the VCA PAW value of the MAE at the maximum is somewhat smaller then in the TB-LMTO ASA calculations by Turek *et al.* [15], $K_u \approx 600$ μeV/atom vs $K_u \approx 800$ μ eV/atom, respectively, it is still almost three times larger than the values obtained with

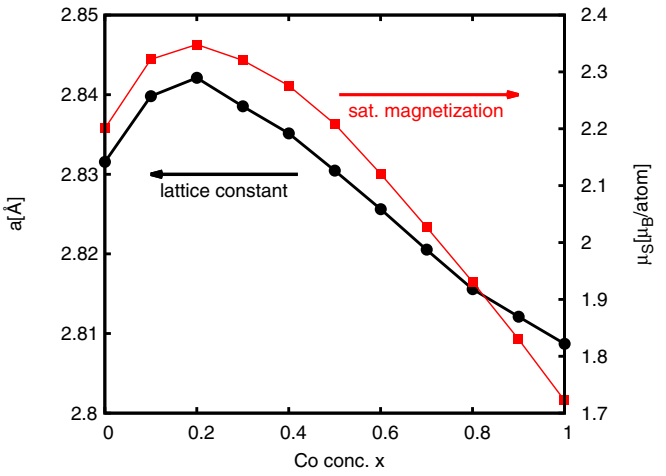

FIG. 1. Left panel: Calculated lattice constants. Right panel: Calculated total magnetic moment, as a function of the Co concentration x. The same trend has been shown experimentally in [35].

more refined methods of chemical disorder treatment (CPA and supercell averaging). Since in this work we cover the entire range of the Fe-Co alloy concentrations, we can conclude more on the general performance of the VCA methodology for the MAE calculations in disordered alloys. Indeed the VCA describes the trend of the MAE with the alloy concentration in Fe-Co qualitatively well (the physical reason for this is well described in [15]). However, it largely overestimates the MAE

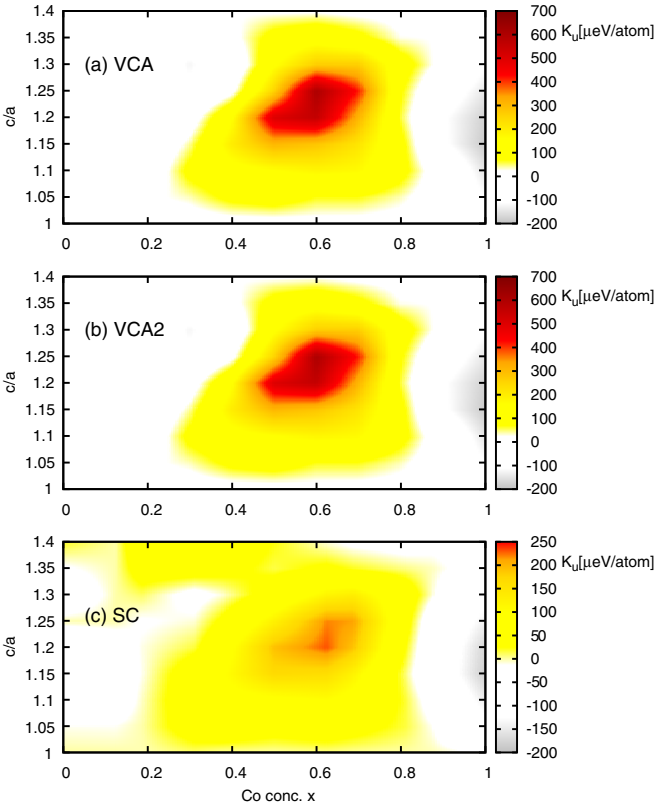

FIG. 2. Calculated uniaxial MAE K_u of tetragonal $Fe_{1-x}Co_x$ as a function of the c/a ratio and the Co concentration x. (a) VCA, (b) VCA2, and (c) supercell calculations.

value almost in all regions of the compositions, except the diluted Co rich regime ($x > 0.85$), see also Fig. 2(c).

We now compare our supercell averaging results to CPA results obtained by Turek *et al.* [15]. We obtain close agreement in the position of the calculated MAE maximum with respect to the c/a ratio and the alloy concentration (around $c/a = 1.25$ and $x = 0.625$) between supercell PAW results and reported CPA calculations. The only difference is that the supercell PAW results give a more extended region of positive anisotropy (easy axis) toward the Co rich region. CPA gives positive MAE values in the range of $0.22 \leqslant x \leqslant 0.65$, whereas the supercell PAW have positive MAE values in the range $0.2 \leqslant x \leqslant 0.8$.

In Fig. 3 we show the calculated MAE as a function of the concentration x for $c/a = 1.2$ and $c/a = 1.25$. In this figure we include the VCA and CPA studies from [15], as well as the available experimental results for $Fe_{0.5}Co_{0.5}$ on the Pd(001) substrate [36] and $Fe_{0.36}Co_{0.64}$/Pt superlattice [8] for $c/a \approx 1.18$. We note the good agreement between the CPA and supercell averaged results. Some small differences might be also related to the fact that the CPA results are derived in the ASA and the LDA. We recall that our VCA values and the TB-LMTO VCA results of [15] showed also some differences that obviously cannot be ascribed to the difference in the treatment of the atomic disorder. Finally, we also observe almost perfect agreement with the experimental results obtained for the MAE for films of tetragonally distorted Fe-Co grown on Pt and Pd substrates. This is also inline with earlier full potential LCAO calculations by Neise *et al.* [16].

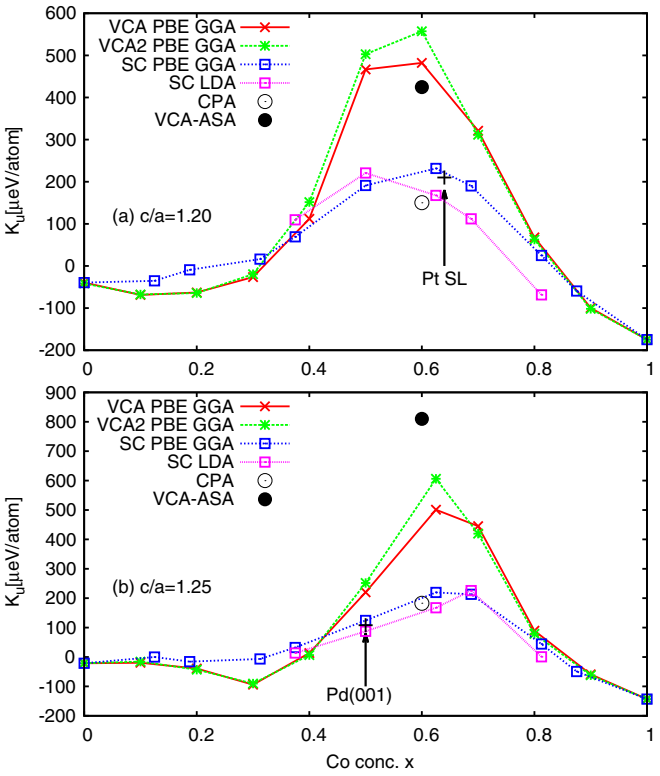

FIG. 3. Calculated uniaxial MAE K_u of tetragonal $Fe_{1-x}Co_x$ as a function of the Co concentration x for VCA, VCA2, and the supercell (SC) results. These were calculated with PBE GGA. Additionally some points were calculated within the supercell method using the LDA. (a) Calculations for $c/a = 1.2$: the black cross indicates an experimental value obtained for $Fe_{0.36}Co_{0.64}$/Pt superlattice [8] for $c/a \approx 1.18$, the black filled circle indicates the VCA-ASA calculations from Ref. [15], and the black open circle indicates the CPA-ASA calculation also from Ref. [15]. (b) Calculations for $c/a = 1.25$: the black cross denotes an experimental value obtained for $Fe_{0.5}Co_{0.5}$ on Pd(001) [36], the black filled circle indicates the VCA-ASA calculation from Ref. [15], and the empty circle the corresponding CPA calculations.

In Fig. 3 we also compare the MAE value derived in GGA and LDA. Interestingly the GGA and LDA results are fairly similar for the Co poor region, but the difference is growing towards the Co rich region. In this region, the LDA yields smaller values than the GGA. Considering the scarcity of experimental results, one cannot draw any definite conclusion in whether GGA or LDA should be preferentially used for the calculation of the MAE in the transition metals alloys.

Overall one might conclude that the simple supercell averaging scheme used in this work for the calculations of the MAE in disordered Fe-Co alloys in combination with the PAW as implemented in VASP performs very well compared to the experiments. The overall agreement between the LDA CPA and the present supercell LDA and GGA calculations is excellent, with the exception of the Co rich region. We will now elaborate on why the results are so sensitive to the computational parameters for the Co rich case. In Fig. 4

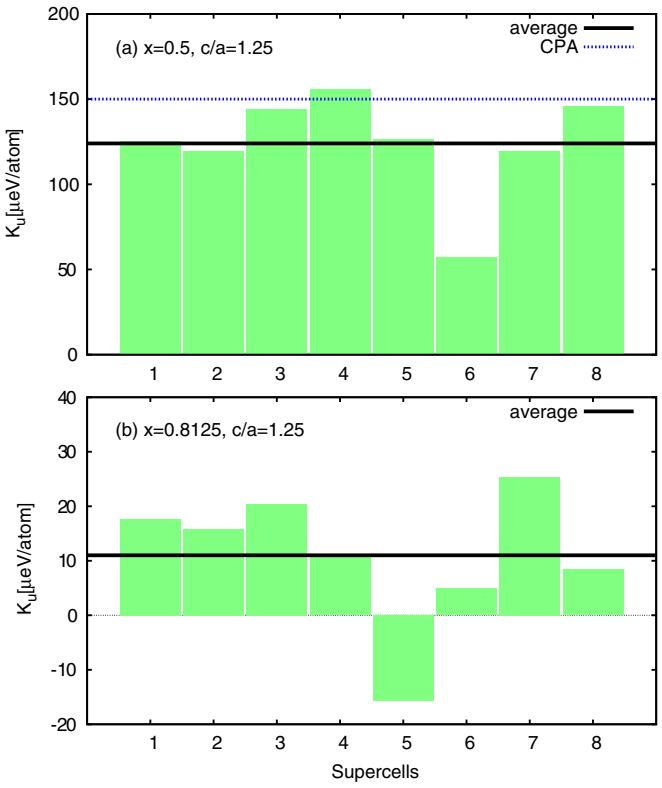

FIG. 4. (a) Calculated uniaxial MAE K_u for tetragonal $Fe_{0.5}Co_{0.5}$ (Fe_8Co_8) and $c/a = 1.25$ for the eight different random supercells. The black solid line denotes the average of the MAE of the supercells. The blue dashed line corresponds to CPA calculations done by Turek *et al.* [15] for $Fe_{0.5}Co_{0.5}$ and $c/a = 1.24$. (b) Calculated uniaxial MAE K_u for tetragonal $Fe_{0.1875}Co_{0.8125}$ (Fe_3Co_{13}) and $c/a = 1.25$ for the eight different random supercells. The black solid line denotes the average of the MAE of the supercells.

we plot the values of the MAE calculated for the individual random supercells used in the averaging. One can see from the upper panel that, in general, the variation of the MAE values calculated for the individual random supercells around the average is not exceeding the difference between the CPA MAE and average supercell MAE. The main difference between CPA and average supercell results is caused, for this particular case, by one supercell (number 6), which has an essentially lower MAE than the rest of the supercells. Thus one would expect the good agreement between supercell averaging and CPA only if the spread in the MAE among supercells is not too large. This condition is relatively well satisfied except for the Co rich case.

The value of the MAE calculated for the individual random supercells for $Fe_{0.1875}Co_{0.8125}$ (Fe_3Co_{13}) alloys are shown in the lower panel of Fig. 4. One can see that in the Co rich region the local environment starts to play a more critical role: SOC on Co is very sensitive to the positions of the only few Fe atoms in the neighboring shells. This causes the relatively strong fluctuations of the single-site Co contribution from negative to positive. In turn, some supercells have negative and some positive MAE [see Fig. 4(b)]. Obviously in this region results are very sensitive to the actual computational parameters and specifically the LDA results differ from the GGA results. We find it rather remarkable that the CPA and the supercell method agree so well even in this region considering that quite different approximations for the one-electron potentials were used in the first-principles CPA methodologies [e.g., atomic sphere approximation (ASA)] and in the PAW (full-potential treatment). In addition, it has been recently demonstrated [37] that there are some differences, at least in the ASA, between the values of the MAE calculated in the framework of the fully relativistic Dirac band structure formalism and perturbational SOC treatments as used in VASP. In summary, the achieved agreement between CPA and the supercell approach is excellent considering these limitations.

V. SUMMARY

The present paper documents how spin-orbit coupling is implemented in the popular first-principles package VASP. The paper therefore fills an important gap in the VASP documentation, as the feature has been distributed and extensively used for almost a decade despite the lack of appropriate documentation.

To evaluate the performance of the implemented spin-orbit coupling within the PAW framework, we have considered calculations of the magnetic anisotropy in tetragonally distorted FeCo alloys. The reason for this choice is that FeCo alloys are simple to calculate, the MAE is fairly large and easy to converge with relatively modest computational setups, and extensive experimental as well as theoretical reference data are available.

We conclude that magnetic anisotropy energies derived within the PAW methodology with spin-orbit coupling are in good agreement with the results of other full potential methods, and for Fe-Co, very well describe the experimental data for tetragonally distorted thin films. Specifically, averaging the MAE calculated for randomly chosen supercells yields results very close to the calculations based on the coherent potential approximation. In the Co rich regime we find the results to be very sensitive to the details of the calculations, with the LDA yielding more negative values for the magnetic anisotropy than the GGA. The previously reported CPA results using the LDA seem to be in between the present LDA and GGA values. Given the sensitivity to the computational parameters, we consider this agreement to be very satisfactory.

ACKNOWLEDGMENT

Support of the Austrian Science Fund (FWF) within the SBF VICOM (F4109N28) is gratefully acknowledged.

[1] D. Weller and A. Moser, IEEE Trans. Magn. **35**, 4423 (1999).
[2] D. Weller, A. Moser, L. Folks, M. Best, W. Lee, M. Toney, M. Schwickert, J. Thiele, and M. Doerner, IEEE Trans. Magn. **36**, 10 (2000).
[3] R. Skomski, P. Manchanda, P. K. Kumar, B. Balamurugan, A. Kashyap, and D. J. Sellmyer, IEEE Trans. Magn. **49**, 3215 (2013).
[4] H. M. Bertram, H. Zhou, and R. Gustafson, IEEE Trans. Magn. **34**, 1845 (1998).
[5] S. H. Charap, P.-L. Lu, and Y. He, IEEE Trans. Magn. **33**, 978 (1997).
[6] W. Kohn and L. J. Sham, Phys. Rev. **140**, A1133 (1965).
[7] G. H. O. Daalderop, P. J. Kelly, and M. F. H. Schuurmans, Phys. Rev. B **44**, 12054 (1991).
[8] G. Andersson, T. Burkert, P. Warnicke, M. Björck, B. Sanyal, C. Chacon, C. Zlotea, L. Nordström, P. Nordblad, and O. Eriksson, Phys. Rev. Lett. **96**, 037205 (2006).
[9] B. Ujfalussy, L. Szunyogh, P. Bruno, and P. Weinberger, Phys. Rev. Lett. **77**, 1805 (1996).
[10] A. B. Shick, F. Maca, and P. M. Oppeneer, Phys. Rev. B **69**, 212410 (2004).
[11] P. Blonski, A. Lehnert, S. Dennler, S. Rusponi, M. Etzkorn, G. Moulas, P. Bencok, P. Gambardella, H. Brune, and J. Hafner, Phys. Rev. B **81**, 104426 (2010).
[12] M. D. Stiles, S. V. Halilov, R. A. Hyman, and A. Zangwill, Phys. Rev. B **64**, 104430 (2001).
[13] T. Burkert, L. Nordström, O. Eriksson, and O. Heinonen, Phys. Rev. Lett. **93**, 027203 (2004).
[14] E. Şaşıoğlu, C. Friedrich, and S. Blügel, Phys. Rev. B **87**, 020410(R) (2013).
[15] I. Turek, J. Kudrnovský, and K. Carva, Phys. Rev. B **86**, 174430 (2012).
[16] C. Neise, S. Schönecker, M. Richter, K. Koepernik, and H. Eschrig, Phys. Status Solidi B **248**, 2398 (2011).
[17] K. Koepernik and H. Eschrig, Phys. Rev. B **59**, 1743 (1999).
[18] S. de Gironcoli, P. Giannozzi, and S. Baroni, Phys. Rev. Lett. **66**, 2116 (1991).
[19] N. Marzari, S. de Gironcoli, and S. Baroni, Phys. Rev. Lett. **72**, 4001 (1994).
[20] A. M. Saitta, S. de Gironcoli, and S. Baroni, Phys. Rev. Lett. **80**, 4939 (1998).

[21] D. Papaconstantopoulos and W. Pickett, Phys. Rev. B **57**, 12751 (1998).
[22] W. E. Pickett and D. J. Singh, Phys. Rev. B **53**, 1146 (1996).
[23] L. Bellaiche and D. Vanderbilt, Phys. Rev. B **61**, 7877 (2000).
[24] G. Kresse and J. Furthmüller, Phys. Rev. B **54**, 11169 (1996).
[25] P. E. Blöchl, Phys. Rev. B **50**, 17953 (1994).
[26] G. Kresse and D. Joubert, Phys. Rev. B **59**, 1758 (1999).
[27] E. van Lenthe, E. J. Baerends, and J. G. Snijders, J. Chem. Phys. **99**, 4597 (1993).
[28] D. Hobbs, G. Kresse, and J. Hafner, Phys. Rev. B **62**, 11556 (2000).
[29] C. Eckhardt, K. Hummer, and G. Kresse, Phys. Rev. B **89**, 165201 (2014).
[30] J. Buschbeck, I. Opahle, S. Fähler, L. Schultz, and M. Richter, Phys. Rev. B **77**, 174421 (2008).
[31] J. P. Perdew, K. Burke, and M. Ernzerhof, Phys. Rev. Lett. **77**, 3865 (1996).
[32] J. P. Perdew and A. Zunger, Phys. Rev. B **23**, 5048 (1981).
[33] S. H. Vosko, L. Wilk, and M. Nusair, Can. J. Phys. **58**, 1200 (1980).
[34] A. I. Lichtenstein, M. I. Katsnelson, V. P. Antropov, and V. A. Gubanov, J. Magn. Magn. Mater. **67**, 65 (1987).
[35] I. Ohnuma, H. Enoki, O. Ikeda, R. Kainuma, H. Ohtani, B. Sundman, and K. Ishida, Acta Mater. **50**, 379 (2002).
[36] F. Luo, X. Fu, A. Winkelmann, and M. Przybylski, Appl. Phys. Lett. **91**, 262512 (2007).
[37] I. Turek, J. Kudrnovský, and K. Carva, J. Supercond. Nov. Magn. **26**, 1581 (2013).